Subcycle characterization of photoelectron emission with multicycle laser pulses

Qinying Ji,[1] Junping Wang,[2] Peifeng Lu,[1] Hui Li,[1] Xiaochun Gong,[1] Qiying Song,[1] Kang Lin,[1] Wenbing Zhang,[1] Junyang Ma,[1] Matthias Friedrich Kling,[3,4] Heping Zeng,[1] Jian Wu,[1,5,*] and Feng He[2,†]

[1]*State Key Laboratory of Precision Spectroscopy, East China Normal University, Shanghai 200062, China*

[2]*Key Laboratory of laser Plasmas (Ministry of Education) and Department of Physics and Astronomy, Collaborative Innovation Center of IFSA (CICIFSA), Shanghai Jiao Tong University, Shanghai 200240, China*

[3]*Max-Planck-Institut für Quantenoptik, D-85748 Garching, Germany*

[4]*Physics Department, Ludwig-Maximilians-Universität Munich, D-85748 Garching, Germany*

[5]*Collaborative Innovation Center of Extreme Optics, Shanxi University, Taiyuan, Shanxi 030006, China*

(Received 7 September 2016; revised manuscript received 16 August 2017; published 30 November 2017)

By partially overlapping two time-delayed orthogonally polarized multicycle laser pulses of the same carrier frequency, we construct an optical waveform whose polarization axis rotates slowly for consecutive optical cycles. This unique laser field tunnel-ionizes atoms and accelerates the freed electrons to different directions at different instants. Classical trajectory Monto Carlo simulations support the resulting angle-resolved photoelectron momentum distribution. Taking advantage of this optical field, we investigate characteristics of electrons triggered by different quarters of an optical cycle and explore the Coulomb focusing effect on electrons traveling along different trajectories. Our experiment using a polarization-skewed near-infrared laser pulse verifies the numerical simulations and demonstrates the feasibility of retrieving subcycle dynamics with multicycle laser pulses.

DOI: 10.1103/PhysRevA.96.053423

I. INTRODUCTION

Photoionization plays a central role in the understanding and steering of ultrafast dynamics in atoms and molecules in strong external laser fields. Plenty of ultrafast processes are directly related to photoionization, including molecular imaging by laser-assisted electron self-diffraction [1,2], high-harmonic generation and attosecond pulse synthetization [3,4], the calibration of the laser carrier-envelope phase [5–7], and laser pulse shape [8,9]. Understanding of photoionization has developed from Einstein's photoelectric effect to multiphoton [10] and tunneling ionization [11]. The capture of ultrafast photoionization processes in real time, accurate to fractions of an optical cycle, has been a long-standing aim for physical chemists.

For multicycle strong infrared laser pulses, each optical cycle distorts the Coulomb potential and produces replicas of tunneling electron wave packets, whose coherent summation results in the discrete above threshold ionization (ATI) energy spectrum of released photoelectrons [10,12]. In this case, it is impossible to identify the wave packet released in a certain optical cycle. To resolve the photoionization within an optical cycle, one possible way is to use a circularly polarized few-cycle infrared laser pulse [13]. Here, the ionization events triggered by different optical cycles will gain distinct momenta since each optical cycle has a different amplitude, and the electrons released within one optical cycle will be angularly streaked into different directions by the rotating laser field [14]. To pick up the ionization events triggered by a multicycle laser pulse using such an angular streaking technique is quite hard since the very similar amplitudes in different cycles will mix up the ionization events released by different cycles in momentum representation. Regardless of the challenge in producing strong isolated attosecond pulses [15,16], the subcycle ionization at selective timing could be initiated with an isolated attosecond pulse in the presence of a near-infrared laser field [3]. Alternatively, some attempts by using orthogonally polarized two-color laser pulses have been reported; in these strategies an electron released by one color is streaked by the other [17–19], or both colors may tunnel-ionize the electron [20–23]. However, the ionization events in a particular optical cycle are still hard to identify, especially for multicycle laser pulses, which are extensively involved in most of the strong-field experiments. The precise determination of the photoionization timing will bring accurate information about ultrafast processes, such as Coulomb explosion [24,25], electron localization [26,27], and electron rescattering [28,29].

In this paper, we conceive a strategy to capture the ionization events in a selected optical cycle of multicycle femtosecond laser pulses. Figure 1(a) shows the superimposed electric fields of two time-delayed multicycle near-infrared laser pulses with the same carrier frequency that are linearly polarized along the y and z axes. In the overlapping region of two pulses, the polarization direction of the combined electric field rotates slowly from the y to the z axis; thus the ionization events triggered by different cycles will be steered into different directions in the polarization plane. The ionization events, initiated in a certain optical cycle, can further be grouped into quarter cycles by the selected photoelectron momentum stripes. The experimental measurements with a polarization-skewed near-infrared laser field validate our proposal and open the possibility to identify the subcycle dynamics with multicycle laser pulses.

II. NUMERICAL MODEL AND SIMULATIONS

For two identical laser pulses linearly polarized along the y and z axes with a central wavelength of 750 nm at an intensity of 1.2×10^{14} W/cm^2, the combined laser field can

*jwu@phy.ecnu.edu.cn
†fhe@sjtu.edu.cn

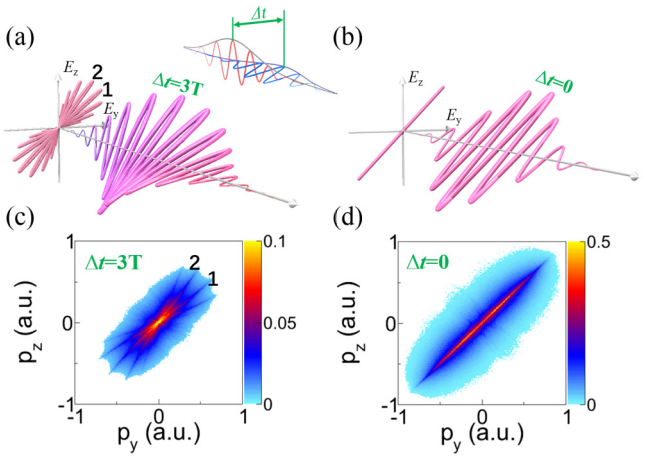

FIG. 1. Laser optical waveforms formed by two overlapping orthogonally polarized ultrashort laser pulses with a time delay of (a) $\Delta t = 3T$ and (b) $\Delta t = 0$, respectively. The inset of (a) shows the definition of the time delay t. (c,d) The corresponding CTMC simulated photoelectron momentum distributions in the polarization plane. The one-to-one correspondence of the stripes between the optical waveform and the observed photoelectron momentum distribution is labeled by "1" and "2" in (a,c).

be expressed as

$$\vec{\mathbf{E}}(t) = E_0\{e^{-2\ln(2)(\frac{t}{\tau})^2}\cos(\omega t+\varphi_0)\overrightarrow{e_y} + e^{-2\ln(2)(\frac{t-\Delta t}{\tau})^2} \times \cos[\omega(t-\Delta t)+\varphi_0]\overrightarrow{e_z}\}, \quad (1)$$

with the amplitude E_0, the temporal duration τ, the carrier frequency ω and carrier-envelope phase φ_0 of the laser field, and the time delay Δt between the two pulses, as shown in the inset of Fig. 1(a). The pulse duration $\tau = 4T$ is applied with T being the optical cycle. In Fig. 1(b), a perfectly linearly polarized laser pulse is formed when $\Delta t = 0$. When $\Delta t = 3T$, as shown in Fig. 1(a), the polarization axis of the combined laser pulses rotates slowly from the y to the z axis and the electric field in each optical cycle orients into different directions. In the overlapping region, the superposed laser electric field is strong and thus provides the main contributions for tunneling ionization.

To demonstrate the feasibility of this strategy, we investigate the photoionization of an argon atom in the polarization-skewed laser field by performing three-dimensional (3D) classical trajectory Monto Carlo (CTMC) simulations. The tunneling picture works for the overlapped laser field according to the Keldysh parameter $\gamma = 1.118$ [30]. At each time step, 10 000 events are sampled in the tunneling exit derived from Landau's effective potential theory [31]. The assembled electrons have a Gaussian-like distribution on the transverse momentum perpendicular to the instantaneous laser field and zero longitudinal momentum along the instantaneous laser field. The sampling electron motion in the combined field of the laser and the Coulomb potential is governed by the Newtonian equation $\ddot{\mathbf{r}} = -\frac{\partial V(\mathbf{r})}{\partial \mathbf{r}} - \mathbf{E}(t)$ where $\mathbf{r}$ is the time-dependent electron displacement from the nuclear core, and $V(\mathbf{r})$ is the modeled Coulomb potential of Ar [32]. Atomic units are used throughout the whole paper unless stated otherwise. After the conclusion of the laser pulse, the three-dimensional asymptotic momenta on virtual detectors are transformed according to the Kepler laws [33]. The final photoelectron momentum distribution (PMD) is obtained by counting all events weighted by the corresponding tunneling ionization rate obtained by the Ammosov-Delone-Krainov (ADK) theory [34,35].

Figures 1(c) and 1(d) present the simulated PMDs obtained from the laser waveforms shown in Figs. 1(a) and 1(b), respectively. As expected, the combined linearly polarized laser field bends the Coulomb potential mainly along the polarization axis; thus the released photoelectrons pile up along 45° in the y-z plane, as shown in Fig. 1(d) for $\Delta t = 0$. The electrons mostly end up with nearly zero momenta along the field direction by being released around the maxima of the laser cycles, which makes it impossible to pick up the photoelectrons emitted from a selected optical cycle. On the contrary, when the time delay is $\Delta t = 3T$, the electric fields of different optical cycles point to different directions, and the projected two-dimensional map of E_y-E_z has a bow-tie shape. The photoelectrons emitted from different optical cycles can be angularly resolved in the polarization plane as shown in Fig. 1(c), sharing similar structures with the laser field in the y-z plane. The one-to-one correspondence of the stripes between the optical field and the observed PMD is labeled by "1" and "2" in Figs. 1(a) and 1(c). Thus, the polarization-skewed laser field allows us to pick out the photoelectrons emitted in a certain optical cycle.

The photoelectron emission within one optical cycle comprises intriguing scenarios. The electrons emitted at different instants may travel along different trajectories and experience different Coulomb actions of the parent ionic core, but reach the same final momenta [36,37]. These kinds of ionization events may induce intracycle interference by forming fork-type structures [38]. In our strategy, after picking out the ionization events induced by a selected optical cycle, we may further identify the roles of each quarter cycle in the photoionization. We plotted the electric field of one optical cycle of the polarization-skewed laser field in Fig. 2(a), and the corresponding PMD in Fig. 2(b). In order to characterize the subcycle photoelectron emission dynamics, we marked the four quarters of the electric field in Fig. 2(a) as Q_1, Q_2, Q_3, and Q_4, respectively. We showed the PMDs contributed by different quarters separately in Figs. 2(c) and 2(d). The final PMDs for Q_1 and Q_3 present a stripe along the laser polarization direction, while the PMDs for Q_2 and Q_4 show a relatively broader momentum distribution.

By looking into the electron trajectories, one may intuitively understand how the Coulomb action of the nuclear core distorts the PMD [39]. For the photoelectron emitted in Q_2, the electrons mainly directly fly away from the parent ion, as shown by a typical trajectory in Fig. 3(b). Therefore, the Coulomb focusing is quite weak for most ionization events. Scenarios are distinct for the photoelectron emission in Q_1. Different from the direct electrons, the rescattering electrons, that first travel outwards and later rescatter with the parent ion [Fig. 3(a)], have been tightly focused by the Coulomb field during propagation, which leads to the well-confined stripe roughly along the laser polarization direction in the PMD. The above analysis has been tested by eliminating the Coulomb potential of the parent ion during the electron propagation, in which case no stripe but dispersive distribution appears. Q_3

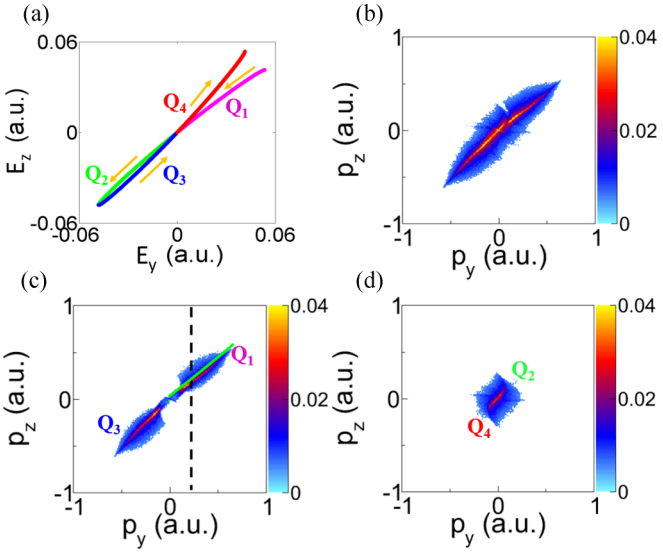

FIG. 2. (a) Temporal evolution of the electric field within an optical cycle of the polarization-skewed laser field, and (b) the CTMC simulated photoelectron momentum distribution released from this particular optical cycle. (c,d) Simulated momentum distribution of the photoelectrons released in given quarter cycles as labeled in (a). The green solid curve represents the negative value of the vector potential, and the vertical dashed line marks the straight (left) and curved (right) PMDs.

and Q_4 also contribute the stripe and dispersive momentum distributions as Q_1 and Q_2, but drive the photoelectron to different momenta.

Besides Coulomb focusing, the Coulomb field of the ionic core also bends the expected photoelectron momentum, which is equivalent to the negative value of the laser vector potential at the tunneling instant [shown by the solid green curve in Fig. 2(c)] if the Coulomb potential is neglected. We calculated the ionization time-dependent momentum deviation between the solid green curve and the CTMC simulated data as $\Delta p(t) = \sqrt{[\langle p_y(t)\rangle + A_y(t)]^2 + [\langle p_z(t)\rangle + A_z(t)]^2}$, which is shown in Fig. 3(c) by the solid black curve. Here $\langle p\rangle$ represents the averaged momentum and only the tightly-Coulomb-focused electrons are included for averaging. For comparison, we analyze the impulse induced by the Coulomb field on the photoelectron by defining $\delta p(t) = \sqrt{\langle \delta p_y(t)\rangle^2 + \langle \delta p_z(t)\rangle^2}$,

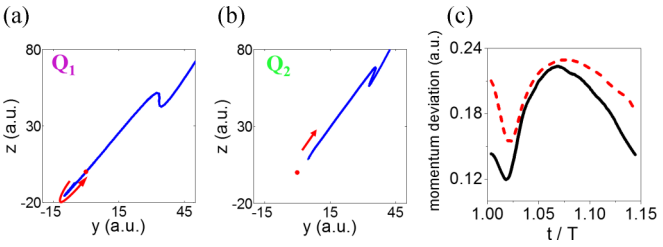

FIG. 3. (a,b) Typical trajectories of the electrons emitted during given quarter cycles labeled in Figs. 2(c) and 2(d). Here the red dot represents the position of the parent core. (c) Momentum deviation caused by the Coulomb potential of the parent core. The dashed red curve is calculated according to the Coulomb impulse, and the solid black curve is obtained from CTMC calculations.

where $\delta p_y(t) = \int_t^{+\infty} dt'(-\frac{\partial V[x(t'),\ y(t'),\ z(t')]}{\partial y})$ and $\delta p_z(t) = \int_t^{+\infty} dt'(-\frac{\partial V[x(t'),\ y(t'),\ z(t')]}{\partial z})$, and show $\delta p(t)$ in Fig. 3(c) by the dashed red curve. Both curves share similar shapes. By tracing the electron trajectories, we find that the combined effect of the initial tunneling exit and the Coulomb field governs the details of the final PMD.

For an ionization time around $t = 1.02T$, we further identify the photoelectron behavior within a quarter optical cycle, whose PMDs are straight and curved, respectively, as shown by the left and right part with respect to the vertical dashed line in Fig. 2(c). This encodes the Coulomb effect of the parent ion on the outgoing photoelectron depending on its initial tunneling exit and subsequent propagation in the laser field as a function of the ionization time. For the electron released at $t < 1.02T$, its tunneling exit increases with the ionization time and the electron undergoes a long trajectory; thus the impulse induced by the Coulomb potential decreases. Around $t = 1.02T$, the initial tunneling exit is larger and the rescattering electron passes the parent core with a relatively large momentum; thus the Coulomb potential acts on the electron within a very short time, leading to the smallest momentum deviation as shown in Fig. 3(c). When the ionization time increases from $1.02T$, the electron does not propagate outwards too much (short trajectory), and thus the electron is embedded by the Coulomb potential before its rescattering. As a result, the momentum deviation increases for the rescattering electron released at $t > 1.02T$. For the electron released at $t > 1.07T$ within a quarter cycle, the tunneling exit as well as the rescattering momentum becomes too large; hence the Coulomb impulse decreases again. Both the Coulomb field strength and the action time determine the momentum deviation.

III. EXPERIMENTAL RESULTS

Inspired by the numerical simulations, we experimentally tested the feasibility of this strategy to distinguish photoelectron emission in different optical cycles. To keep ionization yield by a single pulse negligible and identify the momentum stripes of the photoelectrons produced by the polarization-skewed laser field, two 6-fs (full width at half maximum) laser pulses are used in the present experiments. We used the 6-fs laser pulse instead of the 10-fs pulse used in the simulations because for a shorter laser pulse it is experimentally easier to angularly resolve the photoelectron emission by different optical cycles. As illustrated in Fig. 4(a), a linearly polarized 25-fs laser pulse centered at 790 nm delivered from a Ti:sapphire multipass amplifier is spectrally broadened in a rare-gas-filled hollow core fiber and afterwards temporally compressed into 6 fs using pairs of chirped mirrors. The 6-fs laser beam centered at 750 nm is split into two beams and afterwards recombined using two beam splitters to generate a polarization-skewed optical waveform in a Mach-Zehnder interferometer scheme. The polarization of one laser beam is rotated to be orthogonal to the other using a broadband half-wave plate before their recombination. A similar half-wave plate with optical axis parallel to the light polarization is added in the other interferometry arm to countervail the phase difference between two pulses.

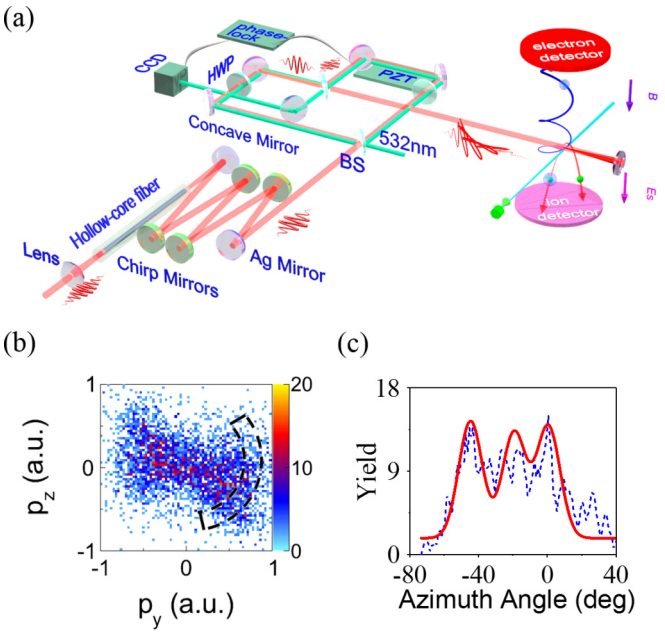

FIG. 4. (a) Schematic view of experimental setup. (b) Measured PMD correlated to Ar^+. (c) The corresponding azimuth angular distribution of the PMD integrated over 0.7 a.u. $< \sqrt{p_y^2 + p_z^2} <$ 0.9 a.u. for $p_y > 0$, indicated by the dashed line in (b). The red curve is the fitting of the measured data to guide the eyes.

The experimental observation of distinct momentum stripes of the photoelectrons requires a spatiotemporally stabilized polarization-skewed optical waveform. It relies on two key issues, i.e., the stabilized carrier-envelope phase φ_0 of the laser pulse and the fixed time delay Δt between two orthogonal pulses. A small change of φ_0 will rotate the whole stripe structure in the polarization plane, while a minor fluctuation of Δt will raise completely different stripe structures of the PMD. The stabilization of the carrier-envelope phase φ_0 of the laser pulse is realized by applying two close loops based on the feedback of the f-2f interferometers [40,41] in both the oscillator and the amplifier of the laser system. The time delay between two pulses is precisely controlled by using a phase-locking system based on the spatial interference of a reference continuum-wave laser beam propagating through the same optical pathways, as illustrated in Fig. 4(a) [42]. Any ineluctable fluctuation of the relative optical path length due to the air flow and mechanical vibration can be compensated by a motorized piezo (PZT) in one arm of the interferometer. In our experiment, the stabilization of φ_0 is better than 250 mrad (root mean square), and the fluctuation Δt is less than 0.1 fs.

The polarization-skewed laser field is afterwards focused onto a supersonic gas jet of Ar atoms by a concave silver mirror ($f = 7.5$ cm) in an ultrahigh vacuum chamber of a cold-target recoil-ion momentum spectrometer (COLTRIMS) [43,44]. The time delay between two orthogonally polarized laser pulses is set to be 2.5T in the current experiment. The intensities of two laser pulses in the interaction region are measured to be $I_{y0} = I_{z0} = 1.5 \times 10^{14}$ W/cm^2, which are estimated by scaling the pulse energy and assuming unchanged focus size and temporal duration of the laser pulse when the polarization is adjusted from linear to elliptical. For elliptically polarized pulses, the peak intensity of the laser field is measured by analyzing the electron momentum distribution in the polarization plane [45]. No ionization of Ar is observed for each single pulse, and the measured photoelectron is mainly produced by the polarization-skewed laser field within the temporal overlap region of the two pulses. The photoionization created electrons and ions are detected by two time- and position-sensitive microchannel plate detectors at opposite ends of the spectrometer. Based on the measured time-of-flights and positions of the impacts, we reconstruct the 3D momenta of the electrons and ions event by event during the offline analysis. Here we focus on the single ionization channel, i.e., $\mathrm{Ar} + m\hbar\omega \rightarrow \mathrm{Ar}^+ + e^-$, for which the law of momentum conservation between the measured electrons and ions is employed along the TOF direction of the spectrometer to select the right events; i.e., $|p_{z,\mathrm{Ar}^+} + p_{z,e^-}| < 0.5$ a.u.

Figure 4(b) displays the measured PMD of the photoelectrons correlated to the Ar^+ in the polarization (y-z) plane. Three obvious stripes would be seen according to the simulated momentum distribution of photoelectrons released for a time delay of 2.5T. The photoelectrons triggered by different optical cycles are angularly resolved along the extending direction of the vector potential curve. As shown in Fig. 4(c), the momentum stripes are more visible by plotting the angular distribution of the PMD integrated over 0.7 a.u. $< \sqrt{p_y^2 + p_z^2} <$ 0.9 a.u. for $p_y > 0$, as shown with the dashed lines in Fig. 4(b). Three peaks in the azimuth angular distribution correspond to the momentum stripes in PMD. This represents an experimental signature of the bow-tie structure of the PMD produced by the polarization-skewed laser field, although the boundaries between the photoelectron momentum stripes are not well distinguished due to the limited resolution of the detector and residual spatiotemporal fluctuations of the optical waveform.

IV. CONCLUSION

In conclusion, we demonstrated that the ultrafast subcycle tunneling ionization dynamics from a selected optical cycle in a multicycle laser field can be resolved by slowly skewing the polarization of the laser field. Compared to isolated attosecond pulses, the polarization-skewed laser pulse can experimentally be prepared much more easily and is strong enough to sustain nonlinear dynamics. Our strategy is robust and can be generalized to many atoms and molecules for the exploration of subcycle dynamics driven by multicycle strong laser fields.

ACKNOWLEDGMENTS

This work is supported by the National Natural Science Fund (Grants No. 11425416, No. 61690224, No. 11621404, No. 11322438, No. 11574205, No. 11327902, and No. 11421064), the 111 project of China (Grant No. B12024), and the Shanghai Sailing Program (Grant No. 17YF1404000), Innovation Program of Shanghai Municipal Education Commission (2017-01-07-00-02-E00034). M.F.K. acknowledges support by the DFG via the excellence cluster "Munich Centre of Advanced Photonics."

Q.J. and J.W. contributed equally to this paper.

[1] C. I. Blaga, J. Xu, A. D. DiChiara, E. Sistrunk, K. Zhang, P. Agostini, T. A. Miller, L. F. DiMauro, and C. D. Lin, Nature (London, U. K.) **483**, 194 (2012).

[2] M. Lein, J. Phys. B **40**, R135 (2007).

[3] M. Hentschel, R. Kienberger, C. Spielmann, G. Reider, N. Milosevic, T. Brabec, P. Corkum, U. Heinzmann, M. Drescher, and F. Krausz, Nature **414**, 509 (2001).

[4] P. M. Paul, E. S. Toma, P. Breger, G. Mullot, F. Aug, Ph. Balcou, H. G. Muller, and P. Agostini, Science **292**, 1689 (2001).

[5] G. G. Paulus, F. Lindner, H. Walther, A. Baltuska, E. Goulielmakis, M. Lezius, and F. Krausz, Phys. Rev. Lett. **91**, 253004 (2003).

[6] T. Wittmann, B. Horvath, W. Helml, M. G. Schätzel, X. Gu, A. L. Cavalieri, G. G. Paulus, and R. Kienberger, Nat. Phys. **5**, 357 (2009).

[7] P. L. He, C. Ruiz, and F. He, Phys. Rev. Lett. **116**, 203601 (2016).

[8] Y. Mairesse and F. Quéré, Phys. Rev. A **71**, 011401(R) (2005).

[9] E. Goulielmakis, M. Uiberacker, R. Kienberger, A. Baltuska, V. Yakovlev, A. Scrinzi, T. Westerwalbesloh, U. Kleineberg, U. Heinzmann, M. Drescher, and F. Krausz, Science **305**, 1267 (2004).

[10] P. Agostini, F. Fabre, G. Mainfray, G. Petite, and N. K. Rahman, Phys. Rev. Lett. **42**, 1127 (1979).

[11] M. Uiberacker, Th. Uphues, M. Schultze, A. J. Verhoef, V. Yakovlev, M. F. Kling, J. Rauschenberger, N. M. Kabachnik, H. Schröder, M. Lezius, K. L. Kompa, H.-G. Muller, M. J. J. Vrakking, S. Hendel, U. Kleineberg, U. Heinzmann, M. Drescher, and F. Krausz, Nature **446**, 627 (2007).

[12] W. C. Wallace, M. G. Pullen, D. E. Laban, O. Ghafur, H. Xu, A. J. Palmer, G. F. Hanne, K. Bartschat, A. N. Grum-Grzhimailo, H. M. Quiney, I. V. Litvinyuk, R. T. Sang, and D. Kielpinski, New J. Phys. **15**, 033002 (2013).

[13] J. Wu, M. Magrakvelidze, L. P. H. Schmidt, M. Kunitski, T. Pfeifer, M. Schöffler, M. Pitzer, M. Richter, S. Voss, H. Sann, H. Kim, J. Lower, T. Jahnke, A. Czasch, U. Thumm, and R. Dörner, Nat. Commun. **4**, 2177 (2013).

[14] J. Itatani, F. Quéré, G. L. Yudin, M. Y. Ivanov, F. Krausz, and P. B. Corkum, Phys. Rev. Lett. **88**, 173903 (2002).

[15] Sh. Zhong, X. He, Y. Jiang, H. Teng, P. He, Y. Liu, K. Zhao, and Z. Wei, Phys. Rev. A **93**, 033854 (2016).

[16] E. J. Takahashi, P. Lan, O. D. Mücke, Y. Nabekawa, and K. Midorikawa, Nat. Commun. **4**, 2691 (2013).

[17] M. Kitzler and M. Lezius, Phys. Rev. Lett. **95**, 253001 (2005).

[18] M. Richter, M. Kunitski, M. Schöffler, T. Jahnke, L. P. H. Schmidt, M. Li, Y. Liu, and R. Dörner, Phys. Rev. Lett. **114**, 143001 (2015).

[19] M. Richter, M. Kunitski, M. Schöffler, T. Jahnke, L. Ph. H. Schmidt, and R. Dörner, Phys. Rev. A **94**, 033416 (2016).

[20] L. Zhang, X. Xie, S. Roither, D. Kartashov, Y. L. Wang, C. L. Wang, M. Schöffler, D. Shafir, P. B. Corkum, A. Baltuška, I. Ivanov, A. Kheifets, X. J. Liu, A. Staudte, and M. Kitzler, Phys. Rev. A **90**, 061401(R) (2014).

[21] X. Xie, Phys. Rev. Lett. **114**, 173003 (2015).

[22] J.-W. Geng, W.-H. Xiong, X.-R. Xiao, L.-Y. Peng, and Q. Gong, Phys. Rev. Lett. **115**, 193001 (2015).

[23] X. Gong, C. Lin, F. He, Q. Song, K. Lin, Q. Ji, W. Zhang, J. Ma, P. Lu, Y. Liu, H. Zeng, W. Yang, and J. Wu, Phys. Rev. Lett. **118**, 143203 (2017).

[24] B. D. Esry, A. M. Sayler, P. Q. Wang, K. D. Carnes, and I. Ben-Itzhak, Phys. Rev. Lett. **97**, 013003 (2006).

[25] Th. Ergler, A. Rudenko, B. Feuerstein, K. Zrost, C. D. Schröter, R. Moshammer, and J. Ullrich, Phys. Rev. Lett. **97**, 193001 (2006).

[26] M. F. Kling, Ch. Siedschlag, A. J. Verhoef, J. I. Khan, M. Schultze, Th. Uphues, Y. Ni, M. Uiberacker, M. Drescher, F. Krausz, and M. J. J. Vrakking, Science **312**, 246 (2006).

[27] D. Ray, F. He, S. De, W. Cao, H. Mashiko, P. Ranitovic, K. P. Singh, I. Znakovskaya, U. Thumm, G. G. Paulus, M. F. Kling, I. V. Litvinyuk, and C. L. Cocke, Phys. Rev. Lett. **103**, 223201 (2009).

[28] W. Becker, X. Liu, P. J. Ho, and J. H. Eberly, Rev. Mod. Phys. **84**, 1011 (2012).

[29] Z.-C. Li and F. He, Phys. Rev. A **90**, 053423 (2014).

[30] L.V. Keldysh, Sov. Phys. JETP **20**, 1307 (1965).

[31] L. D. Landau and E. M. Lifschitz, *Quantum Mechanics (Non-Relativistic Theory)* (Oxford University Press, NewYork, 1958).

[32] X. M. Tong and C. D. Lin, J. Phys. B **38**, 2593 (2005).

[33] N. I. Shvetsov-Shilovski, S. P. Goreslavski, S. V. Popruzhenko, and W. Becker, Laser Phys. **19**, 1550 (2009).

[34] M. V. Ammosov, N. B. Delone, and V. P. Kraĭnov, Sov. Phys. JETP **64**, 1191 (1986).

[35] N. B. Delone and V. P. Krainov, J. Opt. Soc. Am. B **8**, 1207 (1991).

[36] M.-H. Xu, L.-Y. Peng, Z. Zhang, Q. Gong, X.-M. Tong, E. A. Pronin, and A. F. Starace, Phys. Rev. Lett. **107**, 183001 (2011).

[37] D. Comtois, D. Zeidler, H. Pépin, J. C. Kieffer, D. M. Villeneuve, and P. B. Corkum, J. Phys. B: At., Mol. Opt. Phys. **38**, 1923 (2005).

[38] Y. Huismans, A. Rouzée, A. Gijsbertsen, J. H. Jungmann, A. S. Smolkowska, P. S. W. M. Logman, F. Lépine, C. Cauchy, S. Zamith, T. Marchenko, J. M. Bakker, G. Berden, B. Redlich, A. F. G. van der Meer, H. G. Muller, W. Vermin, K. J. Schafer, M. Spanner, M. Yu. Ivanov, O. Smirnova *et al.*, Science **331**, 61 (2011).

[39] D. Shafir, H. Soifer, C. Vozzi, A. S. Johnson, A. Hartung, Z. Dube, D. M. Villeneuve, P. B. Corkum, N. Dudovich, and A. Staudte, Phys. Rev. Lett. **111**, 023005 (2013).

[40] R. Holzwarth, T. Udem, T. W. Hänsch, J. C. Knight, W. J. Wadsworth, and P. S. J. Russell, Phys. Rev. Lett. **85**, 2264 (2000).

[41] D. Jones, S. Diddams, J. K. Ranka, A. Stentz, R. S. Windeler, J. L. Hall, and S. T. Cundiff, Science **288**, 635 (2000).

[42] K. Lin, X. Gong, Q. Song, Q. Ji, W. Zhang, J. Ma, P. Lu, H. Pan, J. Ding, H. Zeng, and J. Wu, J. Phys. B **49**, 025603 (2016).

[43] R. Dörner, V. Mergel, O. Jagutzki, L. Spielberger, J. Ullrich, R. Moshammer, and H. Schmidt-Böcking, Phys. Rep. **330**, 95 (2000).

[44] J. Ullrich, R. Moshammer, A. Dorn, R. Dörner, L. Ph. H. Schmidt, and H. Schmidt-Böcking, Rep. Prog. Phys. **66**, 1463 (2003).

[45] A. S. Landsman, C. Hofmann, A. N. Pfeiffer, C. Cirelli, and U. Keller, Phys. Rev. Lett. **111**, 263001 (2013).